

Performance Comparison between Adjustable Field IPM Motor Based on Permeability Modulation Technique and Conventional IPM Motor

Kiyohiro Iwama
 Graduate School of Integrated Science
 and Technology
 Shizuoka University
 Hamamatsu, Japan
 iwama.kiyohiro.14@shizuoka.ac.jp

Toshihiko Noguchi
 Graduate School of Integrated Science
 and Technology
 Shizuoka University
 Hamamatsu, Japan
 noguchi.toshihiko@shizuoka.ac.jp

Abstract—A proposed adjustable field interior permanent magnet (IPM) motor based on a permeability modulation technique was discussed in this paper. The permeability modulation technique can modulate the permeability of a magnetic material using magnetic saturation with the special magnetic flux. The proposed IPM motor can control an amount of PM flux which interlinks to the stator windings modulating the permeability of the leakage magnetic paths. In this paper, it was confirmed that the proposed IPM motor has superiority of the driving range, the copper loss when driving at the high-speed, and torque ripple over the conventional IPM motor through the several electromagnetic field analyses.

Keywords—permeability modulation, adjustable field, IPM motor, magnetic saturation, zero-phase current

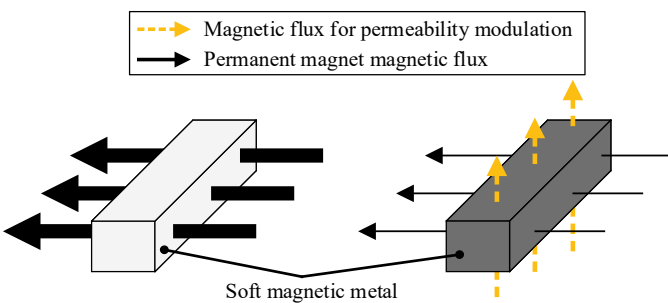
I. INTRODUCTION

In recent years, the PM motors have been used widely because these motors can realize the high output power density in high efficiency. However, it is very difficult to achieve compatibility design of low-speed-high-torque and high-speed-low-torque driving with the PM motor because the magnetic field of the PM is constant. Conventionally, the high-speed driving range of the PM motor has been enlarged utilizing the negative d -axis current. However, it is a problem that the copper loss increases in the high-speed driving range.

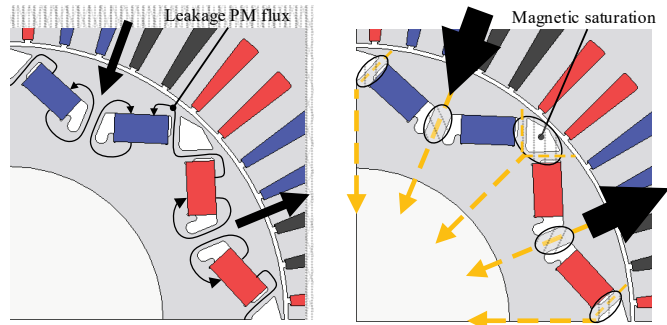
For this reason, the many adjustable field PM motors are focused on [1]-[6]. The adjustable field PM motor which is proposed in reference [1]-[4] can control the magnetic flux density of an air gap utilizing the static magnetic field

generated by the field winding. However, the DC/DC converter to generate the static magnetic field is required in these motors. Therefore, the switching loss of the DC/DC converter and the copper loss of the field winding increase. In addition, these motors cannot output the reluctance torque because these motors are the surface PM motor. Therefore, the output density of these motors is lower than the IPM motor. The adjustable field PM motor proposed in the reference [5] can achieve compatibility of the high-speed-low-torque and low-speed-high-torque driving using the magnetization and the demagnetization of the PM. However, this motor needs the large magnetomotive force (m.m.f.) for the magnetization and demagnetization. Therefore, this motor must control it using the large DC/AC inverter.

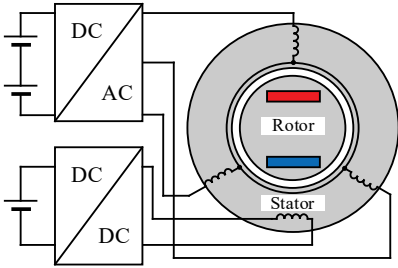
For the above problem, the authors have proposed the new adjustable field method based on the permeability modulation technique^[10]. The adjustable field method using magnetic saturation has been researched in reference [7]. However, this method uses the magnetic flux in the dq -reference frame for magnetic saturation of the leakage magnetic paths. In constant, the proposed method uses the independent magnetic flux penetrating vertically for the dq -reference frame. We also have proposed a 3-phase 4-wire inverter as the motor drive system of the proposed IPM motor. The 3-phase 4-wire inverter can control not only the d -axis current i_d and the q -axis current i_q but also the zero-phase current i_z independently. This motor drive system can adjust the field with only one inverter utilizing i_z as the m.m.f. source for the permeability modulation.



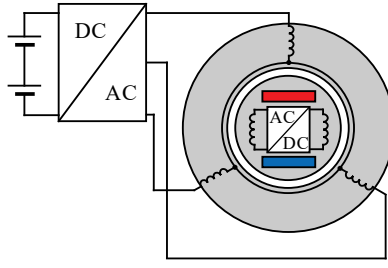
(a) Without magnetic saturation. (b) In case of magnetic saturation.
 Fig. 1. Permeability modulation principle.



(a) Without magnetic saturation. (b) In case of magnetic saturation.
 Fig. 2. Basic principle of proposed adjustable field.



(a) Method using DC/DC converter.



(b) Method using time and/or space harmonics.

Fig. 3. Motor drive circuits of conventional adjustable field PM motor.

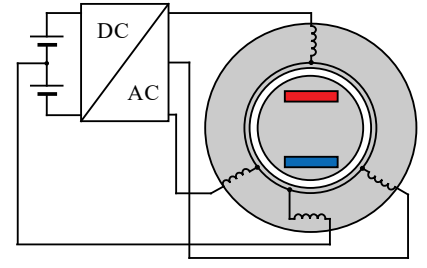


Fig. 4. Motor drive circuit of proposed adjustable field IPM motor.

This paper described the detailed performances of the proposed IPM motor obtained by the electromagnetic field analysis. Besides, these analysis results of the proposed IPM motor were compared with the conventional IPM motor.

II. BASIC ADJUSTABLE FIELD PRINCIPLE BASED ON PERMEABILITY MODULATION TECHNIQUE

A basic principle of the permeability modulation is shown in Fig. 1. As shown in Fig. 1, the main magnetic flux is horizontally penetrating the soft magnetic metal, which is adjusted by the different magnetic flux for the permeability modulation penetrating the soft magnetic metal vertically. By intensifying the magnetic flux for the permeability modulation, the soft magnetic metal is saturated magnetically, and its permeability decreases. As a result, the main magnetic flux penetrating the soft magnetic metal decreases. Therefore, it is possible to control the main magnetic flux amount by modulating the permeability of the soft magnetic metal.

Fig. 2 illustrates an application of the permeability modulation technique described above, which makes it possible to control the leakage magnetic flux between the PM poles. This figure shows a cross-section of the 1/4 model of the proposed IPM motor. The leakage magnetic paths between the PMs are modulated by the magnetic flux for the permeability modulation. As already described, the permeability modulation is carried out by using the differently allocated special winding in the stator in addition to the standard 3-phase windings. Therefore, this special winding is not called the field winding but the modulation winding. As shown in Fig. 2(a), when the leakage magnetic paths are not magnetically saturated, the short magnetic circuits are caused between the PMs. Therefore, the main magnetic flux of PMs hardly interlinks to the stator windings. On the other hand, because the permeability between the PMs decreases due to the magnetic saturation of the leakage magnetic paths, most of the PM flux interlinks to the stator windings, which corresponds to the intensified field control as illustrated in Fig. 2(b). As described above, the proposed strategy achieves the adjustable field control utilizing the permeability variation caused by the magnetic saturation of the leakage magnetic paths between the PMs. Many of the adjustable field approaches give the motor some kinds of electromagnetic energy in the high-speed driving range as presented [1]-[4] and [6]. However, in the proposed adjustable field method, the m.m.f. for the permeability modulation is decreased in high-speed driving range. Therefore, the proposed adjustable field method is completely different from any other approach in the past.

III. DRIVE SYSTEMS OF ADJUSTABLE FIELD IPM MOTOR

A. Drive Systems of Conventional Adjustable Field PM Motor

Fig. 3 shows the motor drive system of the conventional adjustable field IPM motor. The motor drive circuit shown in Fig. 3(a) is used in [1]-[4]. The switching loss increases in this motor drive system because this motor drive system uses the DC/DC converter in addition to the DC/AC inverter. On the other hand, the adjustable field PM motor proposed in [6] uses the motor drive system shown in Fig. 3(b). This motor drive system can utilize the time and/or space harmonics by rectifying these harmonics in the rotor. However, the switching loss increases as with Fig. 3(a) because this motor needs the AC/DC rectifier in the rotor. Furthermore, this motor drive system has drawbacks that the magnetic field is uncontrollable because the time and/or space harmonics increase in proportion to the rotating speed based on Faraday's law.

B. Drive System of Proposed Adjustable Field IPM Motor

The proposed motor drive system is depicted in Fig. 4. As shown in Fig. 4, the proposed IPM motor connected to the 3-phase 4-wire inverter. Therefore, it is possible to control not only the three-phase current but also the i_z . The i_z is utilized as the permeability modulation m.m.f. source. The voltage equation of the proposed motor drive system is as follows:

$$\begin{bmatrix} v_0 \\ v_d \\ v_q \end{bmatrix} = \begin{bmatrix} (R_a + 3R_z) + pL_0 & 0 & 0 \\ 0 & R_a + pL_d & -\omega L_q \\ 0 & \omega L_d & R_a + pL_q \end{bmatrix} \begin{bmatrix} i_0 \\ i_d \\ i_q \end{bmatrix} + \begin{bmatrix} 0 \\ 0 \\ \omega \Psi_f \end{bmatrix}, \quad (1)$$

where the variables and the parameters are defined as

$v_0, v_d,$ and v_q : voltages on the $0dq$ reference frame,

$i_0, i_d,$ and i_q : currents on the $0dq$ reference frame,

R_a and R_z : three-phase and zero-phase winding resistance,

$L_0, L_d,$ and L_q : winding inductances on the $0dq$ reference frame,

p : differential operator, and

ω : angular speed.

From Eq. (1), we can control the i_z using a block diagram shown in Fig. 5. The switching loss of this motor drive system is almost the same as the conventional motor drive system because switching times do not change. Furthermore, the potential level at the neutral point does not vary because the i_z is used as the DC in this proposed adjustable field method.

Therefore, the proposed motor drive system hardly exerts an adverse influence on the power supply voltage availability.

For these reasons, the proposed motor drive system has superiorities about the switching loss and controllability compared with the conventional motor drive systems.

IV. BASIC CHARACTERISTICS OF PROPOSED IPM MOTOR

A. Magnetic Circuit Dseding of Proposed IPM Motor

The proposed adjustable field IPM motor model analyzed with JMAG-designer19.0TM and motor specifications are shown in Fig. 6 and TABLE I, respectively. Both the stator and the rotor core of the proposed motor is split into 2 parts, and the modulation winding is inserted between these stator cores. In addition, the 3-dimensional magnetic circuit is realized because the motor frame and the rotor shaft are made of S45C. Moreover, the rotor skew is applied to the proposed motor to reduce the space harmonics. The rotor skew with a skew angle of 3.75 deg makes it possible to reduce the 6th and the 12th order torque ripple.

Fig. 7 shows the relative permeability distribution provided by only the modulation flux. The modulation m.m.f. F_m of 1200 AT is given to the modulation winding in this analysis. As can be seen from this figure, it is confirmed that the permeability of the leakage magnetic path is 30. The initial relative permeability of the electromagnetic steel sheet which is used as the rotor core is around 5000. From the above simulation result, it can be seen that the proposed IPM motor can modulate the permeability of leakage magnetic paths supplying the F_m .

B. Basic Charateristics of Proposed IPM Motor in No-Load condition

Fig. 8 shows the no-load electromotive force (e.m.f.) waveforms and FFT analysis results in the two cases of the F_m of 0 and 1200 AT. The rotating speed is 3000 r/min in this analysis. According to Fig. 9, when the F_m is not given to the modulation winding, the fundamental component of the no-load e.m.f. is 21.3 V. On the other hand, when the F_m of 1200 AT is given to the modulation winding, the fundamental component of the no-load e.m.f. is 42.1 V. Therefore, the fundamental component of the no-load e.m.f. is adjustable by 49.4%. Moreover, it is confirmed that the odd-number order harmonics except for the 3rd order harmonics are almost not generated. This result is attributed to the rotor skew. From the analysis results, it is confirmed that the proposed IPM motor can control approximately half the magnetic field without the harmonics.

V. PERFORMANCE COMPARISON BETWEEN CONVENTIONAL IPM MOTOR AND PROPOSED IPM MOTOR

A. Basic Charactetistics of Conventional IPM Motor

The conventional IPM motor model to compare with the proposed IPM motor and the specifications of these motors are shown in Fig. 9 and TABLE II, respectively. The magnetic circuit design of the rotor geometry of the conventional IPM

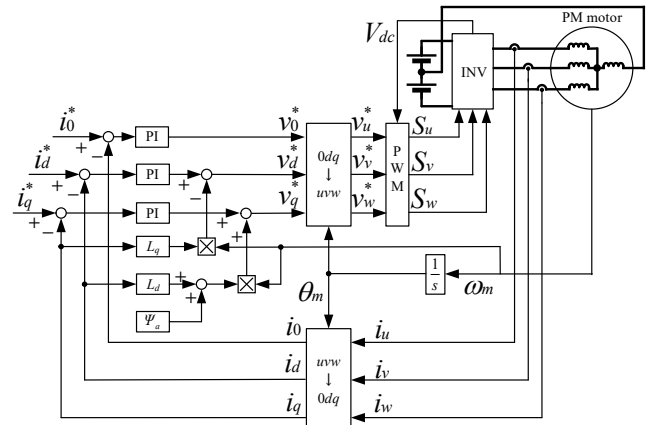


Fig. 5. Block diagram of current controller.

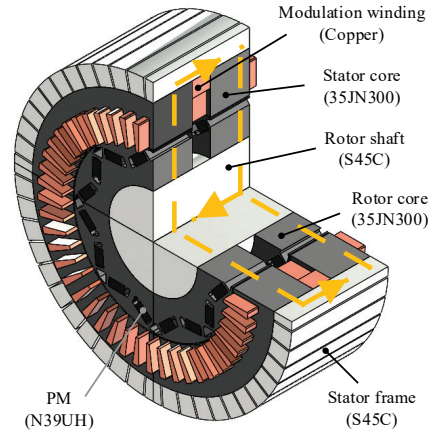


Fig. 6. Proposed adjustable field IPM motor model.

TABLE I. IPM Motor specifications.

Modulation current	10 A_{dc}
Phase current	50 A_{rms}
Current density	20 A/mm^2
Number of poles	8 poles
Number of slots	48 slots
Armature windings	6 turns, 0.158 Ω
Modulation windings	120 turns, 1.800 Ω
Stator diameter	ϕ 148 mm
Rotor diameter	ϕ 96.6 mm
Stack length	62 mm

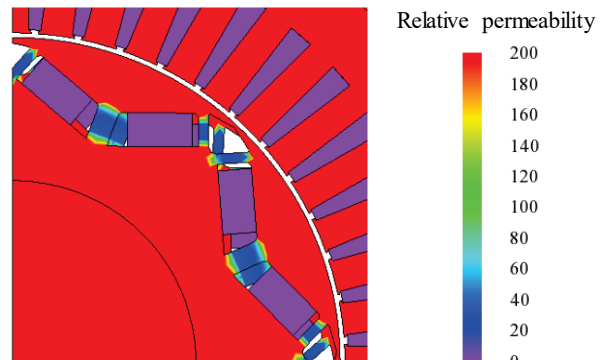
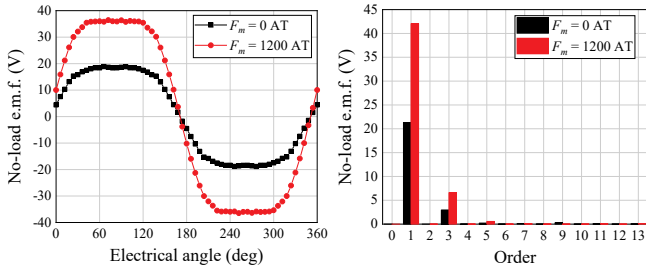
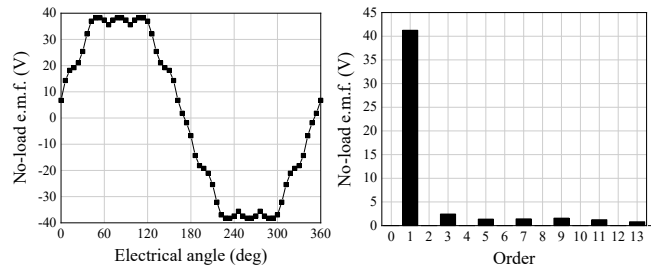


Fig. 7. Counter plot of relative permeability with F_m of 1200 AT.



(a) Waveforms of no-load e.m.f. (b) FFT analysis results of no-load e.m.f.
Fig. 8. No-load e.m.f. of proposed adjustable field IPM motor.



(a) Waveforms of no-load e.m.f. (b) FFT analysis results of no-load e.m.f.
Fig. 10. No-load e.m.f. of conventional IPM motor.

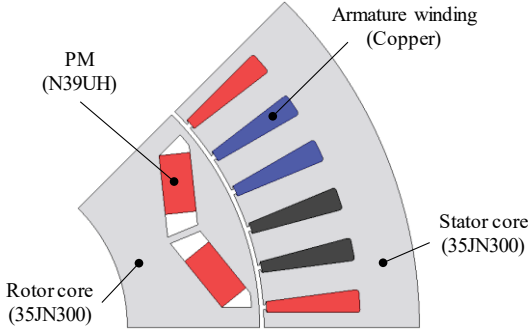


Fig. 9. Conventional IPM motor model.

motor model is made with the reference of the 2nd generation PRIUS released from Toyota Motor Corporation. As can be seen in Fig. 10 and TABLE II, the specifications and materials of the conventional IPM motor is almost the same as the proposed IPM motor. However, the stack length of the conventional IPM motor is slightly smaller than the proposed IPM motor because the modulation winding is inserted in the proposed IPM motor.

Fig. 10 shows the no-load e.m.f. waveform and FFT analysis result of the conventional IPM motor under the same condition as an analysis shown in Fig. 8. However, the no-load e.m.f. of the conventional IPM motor includes the large odd-number order harmonics which are the 5th, the 7th, the 11th, and the 13th order harmonics. The 6th and the 12th order torque ripples are generated by these e.m.f. harmonics.

B. Driving Range Comparison

Fig. 11 shows the driving ranges of the conventional IPM motor and the Proposed IPM motor. The range shown with the black line of Fig. 11(a) is the driving range of the conventional IPM motor carried out the $i_d = 0$ control. Similarly, the blue line of Fig. 11(a) is the driving range of the conventional IPM motor carried out the field weakening control, and the red line of Fig. 11(a) is the driving range of the proposed IPM motor. According to Fig. 11, the comparison results are shown in TABLE III.

TABLE III. Comparison results of driving range.

	Proposed IPM motor	Conventional IPM motor	
		$i_d = 0$ control	Field weakening control
Driving range (p.u.)	1.26	1	1.17
Maximal output power	7.66 kW	6.20 kW	7.70 kW
Maximal speed	21500 r/min	10500 r/min	14000 r/min
Maximal torque	13.3 Nm	14.8 Nm	14.8 Nm

TABLE II. Conventional motor specifications.

	Proposed IPM motor	Conventional IPM motor
Current density	20 A/mm ²	20 A/mm ²
Number of poles	8 poles	8 poles
Number of slots	48 slots	48 slots
Armature windings	6 turns	6 turns
Stator diameter	ϕ 148 mm	ϕ 148 mm
Rotor diameter	ϕ 96.6 mm	ϕ 96.6 mm
Stack length	62 mm	48 mm
Air gap length	0.7 mm	0.7 mm
Magnet shape	5.0 mm \times 9.5 mm	5.0 mm \times 9.5 mm
Magnet volume	36480 mm ³	36480 mm ³

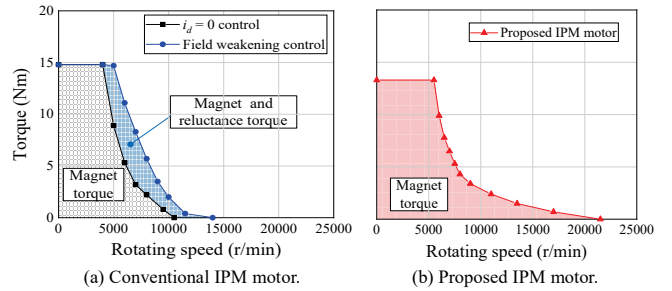


Fig. 11. Analysis results of driving range.

Firstly, the driving range of the proposed IPM motor is compared with the conventional IPM motor carried out the $i_d = 0$ control. These motors do not supply the i_d , and output the only magnet torque. Moreover, when the i_z of 10 A_{dc} and the phase current of 50 A_{rms} is given to the armature winding, the current norm is 86.8 A in the $0dq$ -reference frame. Therefore, these driving ranges shown in Fig. 11 was derived as the maximal current norm in 86.8 A. As can be seen in TABLE III, it is confirmed that the proposed IPM motor has the superiority in terms of the driving range, maximal output, and maximal rotating speed. In particular, the driving range of the proposed IPM motor is larger than the conventional IPM motor by around 26 %.

Secondly, the effects of the field weakening control are considered by making a comparison between the black line and the blue line of Fig. 11. As can be seen from this comparison, The high-speed driving range is expanded by the field weakening control. There are two main reasons for this result. The first reason is the PM flux is weakened by d -axis flux. The second reason is the conventional IPM motor outputs not only the magnet torque but also the reluctance torque. In the following examination, the driving range of the proposed IPM motor is compared with the conventional IPM motor carried out the field weakening control.

C. Copper Loss Comparison

Fig. 12 shows the copper loss map of the proposed IPM motor and the conventional IPM motor. The three driving ranges which are low-speed-high-torque, medium-speed-high-torque, and high-speed-low-torque driving range are considered in the following. The rotating speed is from 0 r/min to 4000 r/min, and torque is from 10 Nm to 15 Nm in low-speed-high-torque driving range. As can be seen in Fig. 12, the copper loss of the proposed IPM motor is slightly larger than the conventional IPM motor because the modulation current is supplied to the proposed IPM motor in this driving range. Moreover, when the rotating speed becomes higher to around 5000 r/min, this gap of the copper loss becomes wide. The field weakening control is applied to the conventional IPM motor in this driving range. Therefore, the conventional IPM motor outputs the high reluctance torque because negative i_d is supplied. For this reason, the conventional IPM motor outputs the high torque with less current than the proposed IPM motor. However, the similar characteristic is expected in the proposed IPM motor because the proposed IPM motor can also output the reluctance torque supplying the negative i_d . Furthermore, the copper loss of the proposed IPM motor is lower than the conventional IPM motor in the high-speed-low-torque driving range. The proposed IPM motor does not supply the modulation current. In constant, the conventional IPM motor supplies the lots of the negative i_d for the field weakening control. Hence, the proposed IPM motor can drive with less current than the proposed IPM motor.

D. Torque Ripple Comparison

The comparison results of the torque ripple factor are shown in Fig. 13. As can be seen in Fig. 13, the torque ripple factor of the proposed IPM motor is lower than the conventional IPM motor all over the driving range. This result is caused by the difference of the odd-number order harmonics of no-load e.m.f. shown in Fig. 8 and Fig. 10. Fig. 14 shows the torque waveforms when both the motor output the equivalent average magnet torque. Because the odd-number order harmonic components of the no-load e.m.f. of the proposed IPM motor is lower than the conventional IPM motor, the 6th and the 12th order torque of the proposed IPM motor are lower than the conventional IPM motor. Moreover, the torque ripple factor of the conventional IPM motor increase in high-speed driving range as illustrated in Fig. 13 (b). Fig. 15 shows the torque waveforms and FFT analysis results when the $i_d = 0$ control and the field weakening control are applied to the conventional IPM motor. As indicated in Fig. 15, both the average torque is equal, and the 12th order torque increases applying the field

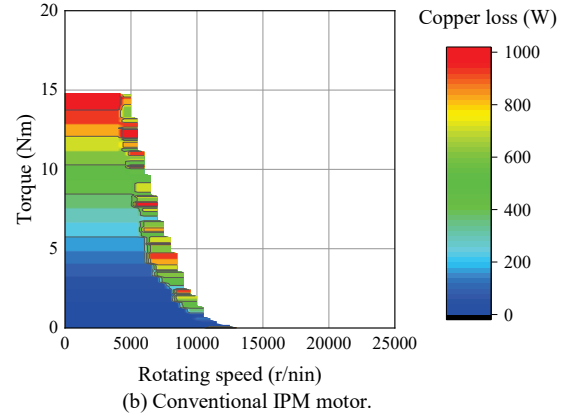
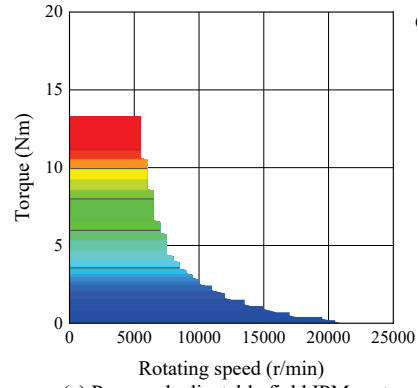


Fig. 12. Copper loss comparison results.

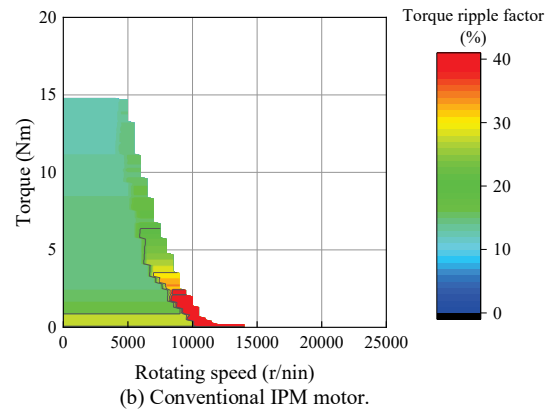
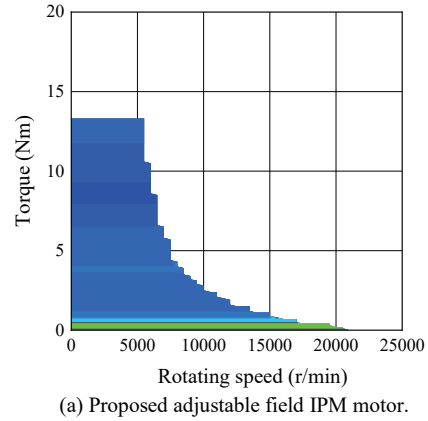
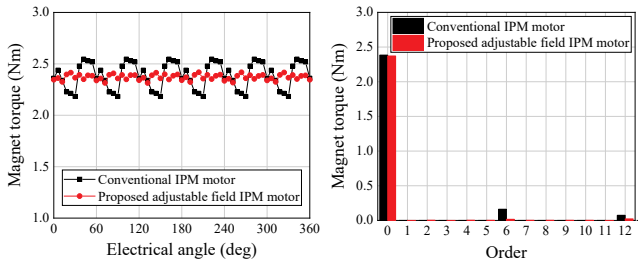
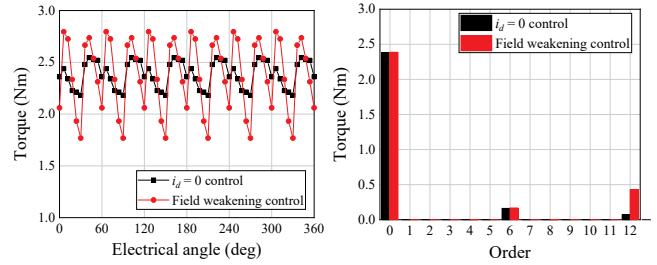


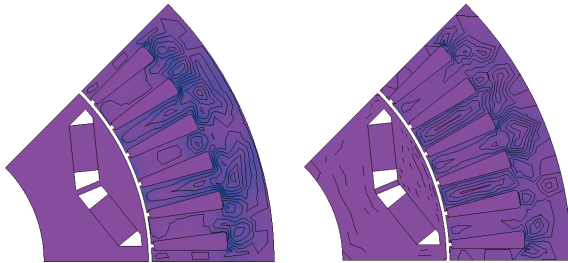
Fig. 13. Torque ripple factor comparison results.



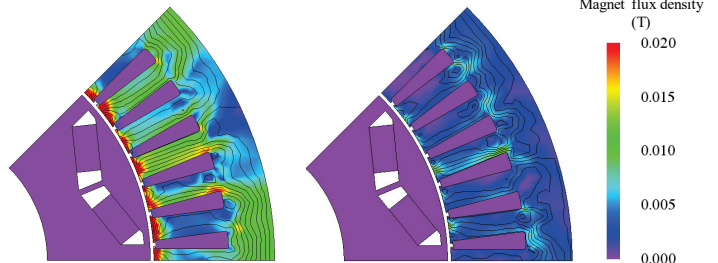
(a) Waveforms of magnet torque. (b) FFT result of magnet torque.
Fig. 14. Analysis results of magnet torque.



(a) Waveforms of torque. (b) FFT result of torque.
Fig. 15. Torque waveforms and FFT analysis results of conventional IPM motor.



(a) 11-th order harmonics. (b) 13-th order harmonics.
Fig. 16. Contour plots of flux density with $i_d = 0$ control.



(a) 11-th order harmonics. (b) 13-th order harmonics.
Fig. 17. Counter plots of flux density with field weakening control.

weakening control. The contour plots of the 11th and the 13th order harmonic armature flux when the 2 controls applied to the conventional IPM motor are shown in Fig. 16 and Fig. 17, respectively. As can be seen from these figures, the 11th and the 13th order harmonic flux increase supplying the negative i_d to the motor. From the above analysis results, the proposed adjustable field method can realize the torque ripple reduction in comparison with the conventional IPM motor.

VI. CONCLUSION

The adjustable field IPM motor based on the permeability modulation technique was proposed in this paper. From the analysis results, it was confirmed that the proposed IPM motor can adjust the magnetic field of 49.4 %. Moreover, the proposed IPM motor was compared with the conventional IPM motor in terms of the driving range, the copper loss, and the torque ripple. Firstly, according to the driving range comparison results, it was thought that the proposed IPM motor has superiority in terms of the driving range and maximal rotating speed. Secondly, judging by the copper loss comparison results, we could see that the copper loss of the proposed IPM motor tends to decrease in high-speed driving range as compared with the conventional IPM motor. Finally, from the torque ripple comparison results, it was confirmed that the proposed IPM motor can reduce the torque ripple compared with the conventional IPM motor.

The future work is confirming the validity of the electromagnetic field analysis results through several experimental verifications.

REFERENCES

- [1] T. Mizuno, K. Nagayama, T. Ashikaga, and T. Kobayashi: "Basic Principles and Characteristics of Hybrid Excitation Type Synchronous Machine," *IEEJ Trans. on IA.*, Vol. 115, No. 11, pp. 1402-1411 (1995)
- [2] M. Namba, K. Hiramoto, and H. Nakai: "Novel Variable-Field Motor with a Three-Dimensional Magnetic circuit," *IEEJ Trans. on IA.*, Vol. 135, No. 11, pp. 1085-1090 (2015)
- [3] T. Ogawa, T. Takahashi, M. Takemoto, H. Arita, A. Daikoku, and S. Ogasawara: "The Consequent-Pole Type Ferrite Magnet Axial Gap Motor with Field Winding for Traction Motor Used in EV," *SAEJ Proc. EVtc & APE Japan 2016*, No.20169094(2016)
- [4] J.A. Tapia, F. Leonardi, and T.A. Lipo: "Consequent-pole Permanent-Magnet Machine with Extended Field-Weakening Capability," *IEEE Trans. on IA.*, Vol. 39, No. 39, pp. 1704-1709 (2003)
- [5] R. Tsunata, M. Takemoto, and S. Ogata: "Investigation of a Variable Flux Memory Motor Using Delta-type PM Arrangement and Extended Flux Barrier for Traction Applications, Ver.1," *IEEJ IA Society Conference*, 3-71, pp.III-408-412 (2019)
- [6] M. Aoyama, K. Nakajima, T. Noguchi: "Proposal and Preliminary Experimental Verification of Electrically Reversal Magnetic Pole Type Variable Magnetic Flux PM Motor," *IEEJ Journal of IA.*, Vol. 7, No. 3, pp. 270-281 (2018)
- [7] T. Kato, H. Hijikata, M. Minowa, Kan. Akatsu, and Robert. D. Lorentz, "Design Methodology for Variable Leakage Flux IPM for Automobile Traction Drives," *IEEE Trans. on IA.*, Vol 51, No. 5, pp. 3811-3821 (2015)
- [8] T.C. Julio: "3D cross coupling effect for flux control in magnetic circuit with Permanent Magnet," *International Symposium on Power Electronics, Electrical Drives, Automation and Motion*, pp. 742-745 (2014)
- [9] Q. Ronghai, M. Aydin, and T.A. Lipo: "Performance comparison of dual-rotor radial flux and axial-flux permanent-magnet BLDC machines," *IEMDC'03. IEEE International*, Vol. 3, pp. 1948-1954 (2003)
- [10] T. Noguchi, K. Iwama, and M. Aoyama: "Adjustable Field PM Motor Based on Permeability Modulation Technique Using Zero-Phase Current," *ICEMS2019* (2019)